Inorganic Chemistry

Article

pubs.acs.org/IC

Survey on the Phase Transitions and Their Effect on the Ion-Exchange and on the Proton-Conduction Properties of a Flexible and Robust Zr Phosphonate Coordination Polymer

Ferdinando Costantino,*[†,‡] Anna Donnadio,[†,§] and Mario Casciola[†]

[†]Dipartimento di Chimica and CEMIN, Via Elce di Sotto n. 8, University of Perugia, Italy

[‡]ICCOM-CNR, Via Madonna del Piano, 10, 50019 Sesto Fiorentino, Florence, Italy

Supporting Information

ABSTRACT: The flexible zirconium tetraphosphonate coordination polymer with formula $Zr(O_3PCH_2)_2N\text{-}C_6H_{10}\text{-}N\text{-}(O_3CH_2P)_2X_{2-x}H_{2+x}\cdot nH_2O$ (X = H, Li, Na, K, $0 < x < 1$, $4 < n < 7.5$) (**1**) possesses an open framework structure with 1D cavities decorated with polar and acids P═O and P—OH groups. **1** has been fully protonated by adding HCl and then subjected to several acid–base ion-exchange reactions with alkaline metals hydroxides. **1** is a very robust coordination polymer because it can be regenerated in H- form using strong acid solutions and ri-exchanged several times without hydrolysis and loss of crystallinity. The flexibility of **1** has been also studied by means of TDXD (temperature dependent X-ray diffraction) evidencing remarkable phase transformations that lead to a different disposition of the water molecules. These transformations also influence the accessibility of the cations on the P—OH groups placed inside the channels and thus the ion-exchange properties. The dependence of the proton conductivity properties on these phase transitions has been also investigated and discussed.

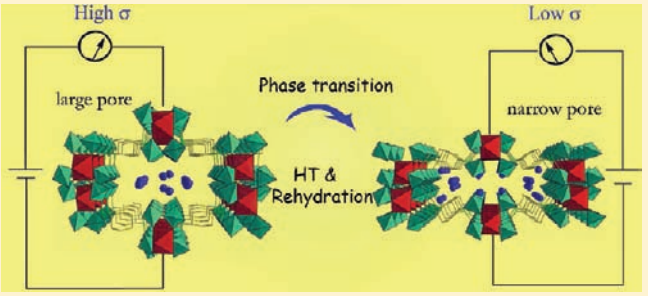

Flexible coordination polymers (coordination polymers = CPs) are three-dimensional hybrid inorganic/organic crystalline solids with open channels that possess a guest-adaptive porosity due to the flexibility of the organic linkers bearing the metal nodes.[1] Remarkable examples of highly flexible porous CPs based on metal carboxylates have been shown, in the last five years, mainly by the Ferey and Kitagawa groups.[2] After a long period dedicated to the synthesis and characterization of the archetypical porous metal–organic framework (MOF), actually scientists' attention is focused on the insertion of functional groups into the pores of the most efficient compounds by using organically modified building blocks[3] or by means of postsynthetic modification,[4] in order to improve the reactivity of the framework in term of sorption, recognition, and catalytic properties.[5] In this context, the synthesis of new stable and robust coordination polymers that could combine a high flexibility with a reactivity easily tunable through the rational choice of the building blocks is considered an ambitious goal. Many authors have recently proposed the insertion of polar and acid groups into the cavities of some of the most known CPs in order to increase the properties related to the acid strength, like the Brönsted acidity and the proton conductivity arising from the mobility of the charge carriers.[6] In the last three years a considerable literature about the proton conduction properties of the carboxylate[7a−d] and phosphonate[7e] based CPs has been yielded. The major part of flexible CPs, based on carboxylic linkers, have the advantage to offer the best control in term of porosity and structural predictability but, on the other hand, all oxygen-based connecting groups are linked to the metal nodes of the SBU (SBU = secondary building units), and therefore, the channels are normally built up only by the organic hydrophobic part. For that reason, the effort for obtaining polar cavities containing acidic groups is normally greater because the use of more sophisticated building blocks or of postsynthetic modifications is required. Porous CPs based on metal phosphonates are less common because the arrangement of the polyphosphonic building blocks is scarcely predictable, and thus, the isoreticular synthesis of porous material is still considered a challenge.[8] On the contrary, they show a higher flexibility and possess a high number of acidic $-PO_3H_2$ groups which are only partly bonded to metal ions, whereas the remaining ones are exposed on the CPs cavities as acid sites. Among metal phosphonates, zirconium derivatives are widely employed because their high insolubility and thermal and chemical stability make them suitable materials for many applications in solid state chemistry like ion exchange, intercalation reactions, and as fillers for polymeric nanocomposites.[9] The major part of zirconium phosphonates has layered or pillared structure, but some derivatives with flexible 3D structure are also reported.[10] The best advantages of CPs based on zirconium phosphonates reside in their very low solubility and high chemical stability that allow us to use them

Received: May 10, 2012
Published: May 29, 2012

   dx.doi.org/10.1021/ic3009656 | *Inorg. Chem.* 2012, 51, 6992–7000

in a wide pH range without dissolution. Some years ago we published the structures of two open framework zirconium phosphonates obtained by using the butyl- and the cyclohexyl-*N,N,N′,N′*-diamino tetraphosphonates as building blocks of formula $(H_2PO_3CH_2)_2N\text{-}C_4H_8\text{-}N(CH_2PO_3H_2)_2$ ($\mathbf{H_8L^1}$) and $(H_2PO_3CH_2)_2N\text{-}C_6H_{10}\text{-}N(CH_2PO_3H_2)_2$, respectively ($\mathbf{H_8L^2}$)[11] whose molecular structures are depicted in Scheme 1.

Scheme 1. Molecular Structures of H_8L^1 and H_8L^2 Tetraphosphonates

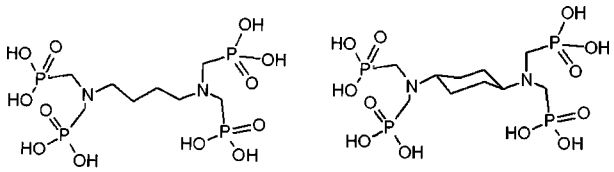

The Zr derivative of $\mathbf{H_8L^2}$, with formula $Zr(O_3PCH_2)_2N\text{-}C_6H_{10}\text{-}N(O_3CH_2P)_2Na_2H_2\cdot 5H_2O$ or $Zr(O_3PCH_2)_2N\text{-}C_6H_{10}\text{-}N(CH_2PO_3)_2(NH_4)_2H_2\cdot 5H_2O$ (hereafter **1_lp@Na** or **1_lp@NH$_4$**, lp for "large pores") possesses a 3D open-framework structure made of inorganic polymeric units bridged by cyclohexyl groups in a "brickwall-like" building texture, as shown in Figure 1. **1** has been prepared in different forms by

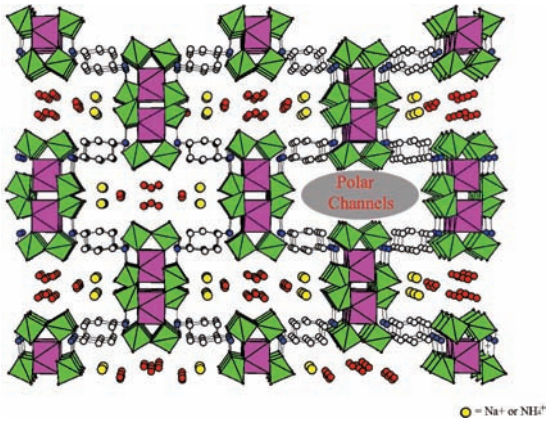

Figure 1. Polyhedral representation, along the *c*-axis, of the structure of **1_lp@(NH4/Na)**.

substituting the cations with H^+ and then re-exchanged with alkaline metals hydroxyde solutions. In this paper the structural flexibility of **1** as consequence of different thermal treatments has been studied by means of TDXD (temperature dependent X-ray diffraction). The ion-exchange properties toward several alkaline metals, with a special attention to lithium, are also discussed. Compound **1** is a good proton conductor: its conductivity properties are based on a Grotthuss mechanism mediated by the water molecules placed into the channels and, for this class of materials, is among the highest. Moreover, the very high insolubility of **1**, with respect to the carboxylate based MOF, can be considered a value added because this allows to use it in a wide pH range. Finally, another important aim of this work concerns the understanding of the relationships that exist between the structural transformation induced by the flexibility of the framework and the changes of the conductivity properties.

EXPERIMENTAL SECTION

Synthesis. Phosphonic acid $\mathbf{H_8L^2}$ was prepared according to the Moedritzer–Irani method.[12]

1_lp@NH$_4$ has been prepared as follows: $ZrOCl_2\cdot 8H_2O$ (0.64 g, 2 mmol) was dissolved in 4 mL of HF 2.9 M and 6 mL of water. This solution was mixed to a 30 mL water solution containing $\mathbf{H_8L^2}$ (1.07 g, 2 mmol) and NH_3 (4 mmol). The reaction mixture was maintained at 80 °C for 3 days in a closed Teflon bottle. The white solid formed was separated by centrifugation, washed three times with water, and dried in air. The fully protonated phase **1_lp@H** was obtained by washing for centrifugation about 300 mg of **1_lp@NH$_4$** with 20 mL of HCl 0.2 M in order to exchange all NH_4^+ or Na^+ ions with H^+. Each washing procedure was repeated 5 times. General formulas of 1 can be written as $Zr(O_3PCH_2)_2N\text{-}C_6H_{10}\text{-}N(O_3CH_2P)_2X_{2-x}H_{2+x}\cdot nH_2O$ (X = H, NH_4, Li, Na, K, $0 < x < 1$, $n = 4–7.5$). For the fully protonated phase X = H, $x = 0$, and $n = 5$. Analysis: calcd. for $ZrNa_2P_4O_{17}N_2C_{10}H_{30}$ (found) Zr, 12.82 (12.75); P, 17.44 (17.30): Na, 6.47 (6.33)

Table 1 shows the formulas for all of the phases.

Table 1. Labelling Scheme, Formulas, and Analysis of 1_lp Phase Samples

phase	formula (from TG data and ICP analysis)	ICP analysis
1_lp@H	$Zr(O_3PCH_2)_2N\text{-}C_6H_{10}\text{-}N(O_3CH_2P)_2H_4\cdot 5.5H_2O$	
1_lp@Na	$Zr(O_3PCH_2)_2N\text{-}C_6H_{10}\text{-}N(O_3CH_2P)_2Na_2H_2\cdot 5H_2O$	Na/Zr = 1.92
1_lp@NH$_4$	$Zr(O_3PCH_2)_2N\text{-}C_6H_{10}\text{-}N(O_3CH_2P)_2(NH_4)_2H_2\cdot 5H_2O$	

Physical Measurements. Coupled thermogravimetric differential thermal analysis (TG-DTA) measurements were performed using a Netzsch STA490C thermoanalyser with a heating rate of 10 °C min^{-1} under a 20 mL min^{-1} air flux.

Titration curves of solids were obtained with a radiometer automatic titrimeter (TIM900Titrliab and ABU91 buret) operating at equilibrium point method on about 100 or 150 mg of samples and using 0.1 M solution of alkaline metal hydroxides. X-ray powder diffraction (XRPD) patterns for structure determination and Rietveld refinement of the compounds were collected according to the step scanning procedure with the Cu Kα radiation on a Philips X'PERT PRO diffractometer, equipped with the X' Celerator solid state fast detector in the 3–100° 2θ range and with 30 s/step counting time. Thermodiffractometric analysis was performed under air with an Anton Paar HTK 1200N hot chamber mounted on a Philips XPERT APD 3020 diffractometer in the 25–160 °C temperature range. Na, Li, K, Zr, and P analyses were performed by Varian 700-ES series Inductively Coupled Plasma-Optical Emission Spectrometers (ICP-OES) Varian Liberty Series II instrument working in axial geometry, after mineralization of samples with mixtures of hydrochloric and nitric acid. Conductivity measurements were carried out on pellets of pressed powder by impedance spectroscopy with a Solartron Sl 1260 Impedance/Gain phase Analyzer in the frequency range 30 kHz–1 MHz at a signal amplitude ≤100 mV. Pellets, 10 mm in diameter and 1–1.5 mm thick, were prepared by pressing ≈200 mg of material at 40 kN/cm^2. The two flat surfaces of the pellet were coated with a thin layer of pressed platinum black (Aldrich) mixed with the powder in the ratio 3:1. The impedance data were fitted to a suitable equivalent circuit by the Zview 2 software (Scribner Associates, Inc.). Details on the complex impedance equation used for curve fitting are reported in the Supporting Information (SI). The pellet conductivity was determined at 70 °C as function of relative humidity (RH) in the range 60–95% and at 95% RH as a function of temperature between 30 and 80 °C. Relative humidity (RH) was controlled as described previously.[13] All the conductivity values here reported refer to measurements carried out after the conductivity had reached a constant value for at least 2 h.

XRPD Structural Analysis Procedures. Cell parameters of the new phases found (**1_np@H** and **1 _an**) were determined by

dx.doi.org/10.1021/ic3009656 | Inorg. Chem. 2012, 51, 6992–7000

autoindexing procedures using the TREOR program.[14] For the phase **1_np@H**, water molecules position was found with the Fourier calculation and their occupancy factor was set according to the TG data (4.5 molecules per formula unit for **1_np@H**). The cell parameters of the phases exchanged with alkaline metal have been found with a LeBail refinement by using the GSAS program.[15] First, zero shift, cell parameters, background, and profile shape parameters were refined. A corrected pseudo Voigt profile function (six terms) with two terms for the correction of asymmetry at the low-angle region was used.

RESULTS AND DISCUSSION

Structural Transformation and Thermal Behavior. The channels of **1_lp** have rectangular shape with dimensions of about 12 Å × 5 Å (calculated perpendicularly to the *c*-axis and between atomic centers). These channels are occupied by five water molecules and by two Na^+ or NH_4^+ ions per formula unit. These guest species are partially hydrated, and the water molecules form a number of strong interactions and H- bonds with each other and with the framework P−O groups. Each cavity possesses eight PO_3C tetrahedral groups pointing toward the inner space. Figure 1 shows the polyhedral representation of **1** whereas Figure 2a shows an enlargement of a single

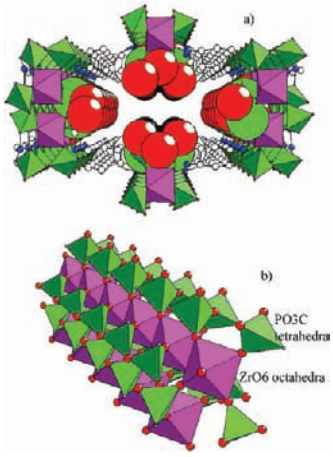

Figure 2. Detail (in van der Waals radii representation) of the P−O/−OH groups pointing inside the cavities (a) and of the connectivity of the composite inorganic building unit of **1** (b).

channel, in which the polar P═O/P—OH groups are represented by using their van der Waals radii. Figure 2b shows a detailed view of the inorganic polymeric units in which the ordered arrays of tetrahedral PO_3C groups can be evidenced. These groups are placed at about 4 Å each other along the *c*-axis.

The electroneutrality requires four acid PO−H groups per formula unit. From the synthesis, these protons are partially exchanged with the Na^+ or NH_4^+ ions that come from NaOH and NH_3 used for the dissolution of the phosphonic acids.

The substitution of Na^+ or NH_4^+ with H^+ induced a remarkable structural flexibility of the framework because of the removal of the intercalated cations into the channels. As a matter of fact, when heated above 150 °C, **1_lp@H** undergoes successive structural transformations due to the water molecules loss, as shown in the temperature dependent X-ray patterns (Figure 3). The same transformations cannot be observed with the Na^+ or NH_4^+ phases because the cations have the effect to retain water and to template the structure. A

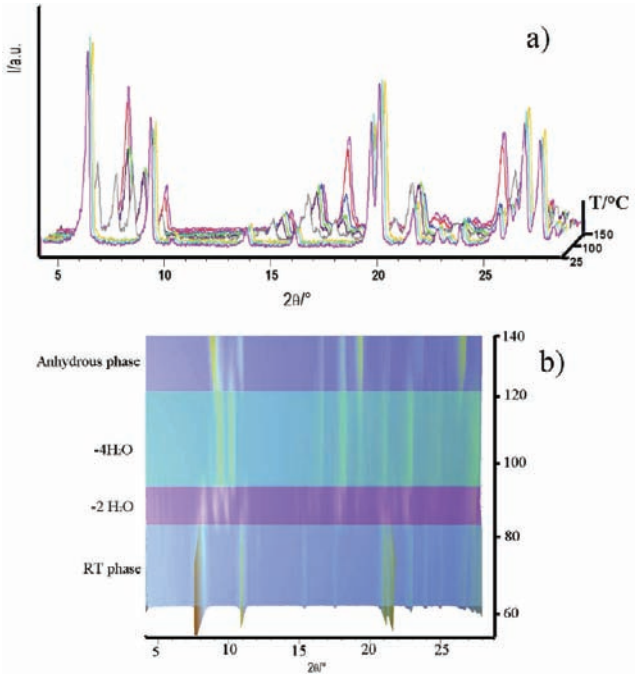

Figure 3. TDXD of **1_lp@H** up to 140 °C: (a) 3D view, (b) isolines view.

further investigation on this effect has been studied for the Li-exchanged phases (see ion-exchange paragraph).

At 150 °C the anhydrous phase is obtained (hereafter **1_an**). The indexation of this powder pattern, achieved by combining the TREOR program and a LeBail profile refinement, gave as result a monoclinic cell with the following parameters: *a* =23.531(5), *b* = 10.862(2), *c* = 8.106(2) Å, *β* = 97.80(4)°, vol = 2052.6(7) $Å^3$ (unfortunately the presence of the peaks belonging to the pristine phases in the XRPD patterns precluded the structural refinement of the anhydrous phase, see the Supporting Information). Despite of the absence of a structural model, the unit cell found could be considered reliable. As a matter of fact, the correlation between the cell parameters of **1_lp@H** (*a* = 18.454, *b* = 16.925, *c* = 7.932 Å, *β* = 92.21°, vol = 2475 $Å^3$) and those of **1_an** indicated that a remarkable contraction of the channels volume, after the guest molecule removal, occurred (about 15.3%). Surprisingly, if the anhydrous phase **1_an** is put in water for few minutes, or left standing at air for 3−4 days, a new phase is formed (XRPD patterns of Figure 3e) with the following cell parameters: *a* = 23.038(1), *b* = 13.1094(7), *c* = 7.6853(4) Å, *β* = 98.349(3)°, vol = 2296.5(1), $Å^3$ (M(20) = 30). In this case, the XRPD pattern shows few and weak impurity lines, and thus, the structure was solved and refined (see the SI for the complete crystallographic data). The results indicate the formation of a new hydrated, fully protonated phase containing about 4.5 water molecules (see TG data in the SI), hereafter called **1_np@H** (**np** for "narrow pore"). For this phase, the relative contraction respect to **1_lp@H** is about 8%.

Figure 4d, e, and f show the Rietveld plots for **1_lp@H**, **1_np@H**, and **1_an** (a detailed view of the plots can be found in the SI). The position of the water molecules in **1_np@H**, found from Rietveld refinement, is slightly different from that of **1_lp@H**. Very likely the regeneration in water of the anhydrous phase induced the formation of new stronger H-bonds between the P−O groups into the channels, that

dx.doi.org/10.1021/ic3009656 | *Inorg. Chem.* 2012, 51, 6992−7000

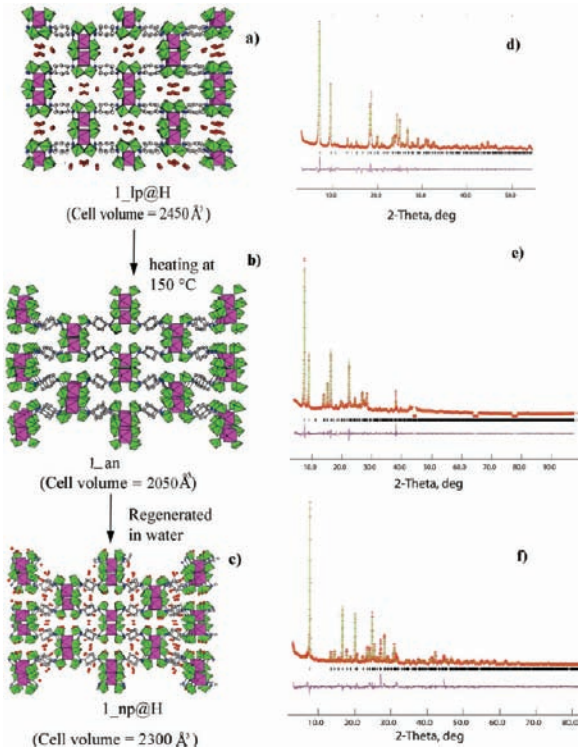

Figure 4. Structure representation and corresponding Rietveld plots for **1_lp@H** (a), **1_an** (b), and **1_np@H** (c). Note that **1_lp@H** and **1_np@H** are full crystallographic structures whereas **1_an** is only a possible structural model based on the cell parameters.

constrain the water molecules to occupy different positions. Indeed, with respect to **1_lp@H** phase, in **1_np@H** the water molecules are placed in the external parts of the channels. The comparison between the structures of **1_lp@H**, **1_an**, and **1_np@H** is shown in Figure 4a, b, and c, left.

Figure 5 shows a detailed view of the channels before and after heating. The transformation paths are also indicated. It

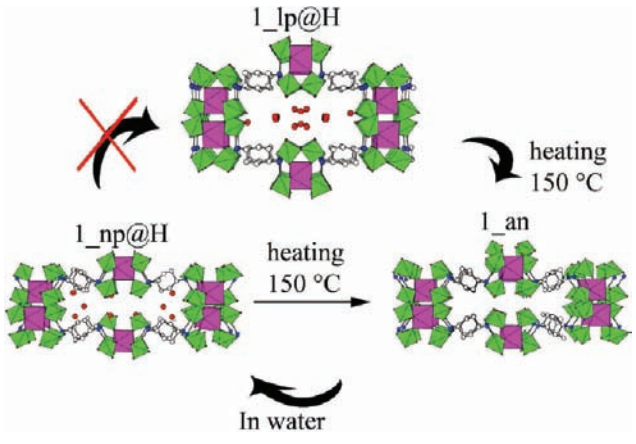

Figure 5. Structural relationships and reactions pathways for **1_lp@H**, **1_an**, and **1_np@H** phases.

can be noticed that the phase **1_lp@H** cannot be regenerated in any way, after **1_np@H** has been formed. This suggests that the latter is the most stable phase although it is obtained after a thermal treatment.

The new position occupied by the water molecules in the **1_np** phase could be also explained with a little rotation of the tetraphosphonate building blocks after heating, that constraint the polar P−O groups to point toward the external part of the channels and thus to create a sort of hydrophilic region where the water molecules can find place, as depicted in Figure 6

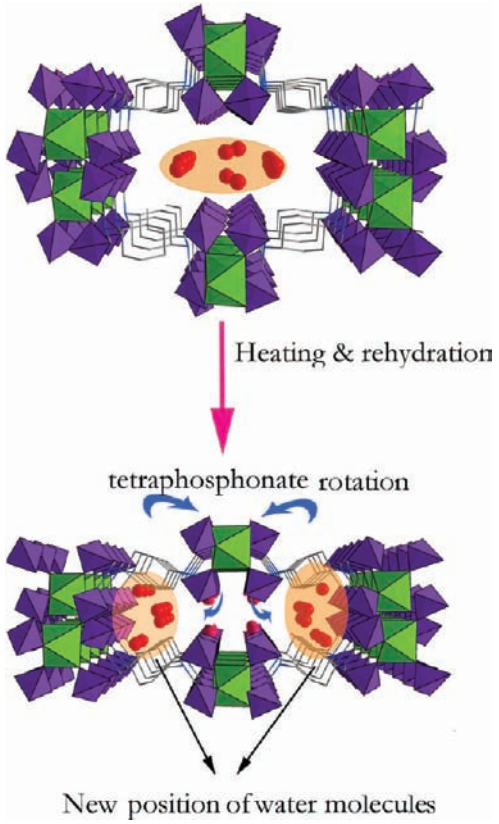

Figure 6. Rotation of the tetraphosphonic groups after heating and new position of the water molecules.

Ion Exchange Properties. Theoretical ion exchange capacity (iec) of **1_lp@H** is about 5.8 meq/gram that is comparable to the best performing layered ion exchangers like α-Zr phosphate (iec of about 6.4 meq/gram).[8] Ion exchanged phases **1_lp@Li**, **1_lp@Na**, **1_lp@K**, and **1_np@Li**, **1_np@Na** have been obtained by titrating 100 mg of both phases **1_np@H** and **1_lp@H** with 0.1 M M−OH solutions (with M = Li, Na, and K) after equilibrating the solids in the respective 1 M metal chloride solutions. The titration of the phase **1_lp@H** with the Na and Li hydroxides in the corresponding metal chloride solution is shown in Figure 7.

The starting pH value is quite low (about 2 or 3) for the two curves suggesting, in a qualitative way, that PO−H groups have high acidity and that a partial substitution of the protons with the alkaline metals occurs just before adding the hydroxide solutions. For Na^+ exchange, the pH slowly grows by increasing the amount of titrating salt. For Na^+ it is possible to evidence an inflection point when 2 mol of hydroxide/mol of compound has been added. This point should correspond to the end of Na^+ uptake. Li^+ shows a more conventional curve in which the protons are exchanged at low pH, as shown by the initial plateau. For Li^+, the inflection point is placed around 1 mol of hydroxide/mol of compound. From the curves it could be inferred that about 2 mol of Na^+ per mol of compound can be exchanged whereas for Li an exchange capacity of about 1 mol of Li^+ per mol of compound is observed. Very likely, the lower

dx.doi.org/10.1021/ic3009656 | Inorg. Chem. 2012, 51, 6992−7000

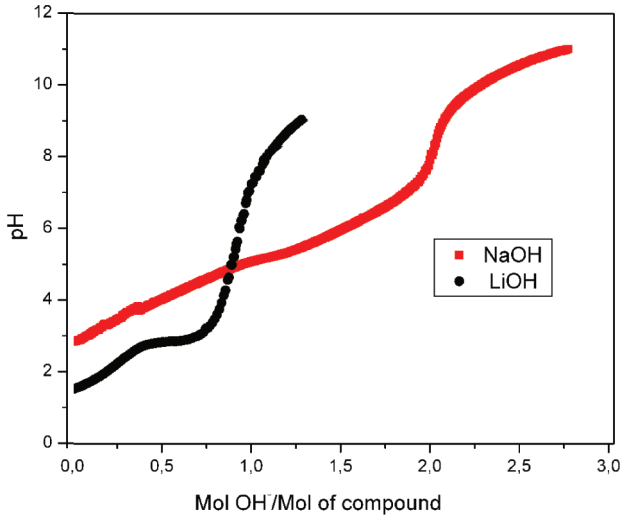

Figure 7. Titration curves for **1_lp** with Li and Na hydroxides 0.1 M solutions in 1 M solution of corresponding chloride salts.

Li^+ uptake, in comparison with that of Na^+ can be ascribed to a higher hydration degree due to the high charge/radius ratio of Li^+. The titration with KOH (shown in the SI) evidenced a different behavior in which pH is a linear function of the amount of added hydroxide. This suggests that K^+ ions enter into the channels at growing energy at every point with a modification of the solid. At the end of titration 1 mol of K^+/mol compound has been found by ICP analyses (see Table 2). The titration with the two hydroxide solutions was also performed on the phase **1_np@H** in the same conditions.

Table 2. Labeling Scheme and Formulas of Exchanged Phases

phase	formula from ICP and TG data	molar ratios (ICP-OES)
1_lp@Li	$Zr(O_3PCH_2)_2N-C_6H_{10}-N(O_3CH_2P)_2LiH_3\cdot 7.5H_2O$	Li/Zr = 1.2
1_lp@Na	$Zr(O_3PCH_2)_2N-C_6H_{10}-N(O_3CH_2P)_2Na_2H_2\cdot 5H_2O$	Na/Zr = 1.92
1_lp@K	$Zr(O_3PCH_2)_2N-C_6H_{10}-N(O_3CH_2P)_2KH_3\cdot 6H_2O$	K/Zr = 0.94
1_np@H	$Zr(O_3PCH_2)_2N-C_6H_{10}-N(O_3CH_2P)_2H_4\cdot 4.5H_2O$	
1_np@Li	$Zr(O_3PCH_2)_2N-C_6H_{10}-N(O_3CH_2P)_2LiH_3\cdot 7H_2O$	Li/Zr = 1.02
1_np@Na	$Zr(O_3PCH_2)_2N-C_6H_{10}-N(O_3CH_2P)_2NaH_3\cdot 4.5H_2O$	Na/Zr = 1.10

In Figure 8, the titration of the phase **1_np** with NaOH is shown. Surprisingly the curve shapes are modified with respect to that of the **lp** phase: the pH grows rapidly to a value of about 5.5, then a plateau is observed and it ends after the exchange of about 0.75 mol of cation/mol of compound. Titration with K^+ was not successful probably because this cation is too large to fit into the channels of the **np** phase. Table 2 shows the molar ratio between Zr and the exchanged alkaline ions for the **1_np** and **1_lp** phases found by ICP analysis.

These observations suggest that the transformation of the phase **1_lp@H** to **1_np@H** is accompanied to a reduction of pores opening that also influences the cation accessibility and thus the energy required to exchange the acid protons. The effect of metal insertion on the structures of **1_lp** and **1_np** phase has been evaluated by means of LeBail refinements on

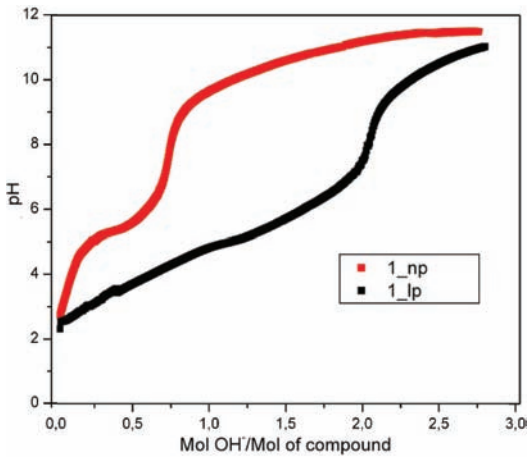

Figure 8. Differences in the titration curves with NaOH for **1_lp** and **1_np**.

the corresponding XRPD patterns and the refined cell parameters are shown in Table 3. The LeBail plots, with the respective agreement indices, are shown in the SI.

The good quality of the fits and the low values of the standard deviations calculated on the cell parameters of all the phases after exchange can be considered a further proof of the chemical stability of this compound in acid and basic conditions.

Notably, the Li- exchanged **1_lp** and **1_np** phases have the higher cell volumes: the *a*- axis, in **1_np** remains similar to that of anhydrous phase (22 Å) whereas the *b*- axis increases until 15 Å that is about 2 Å higher than that of H- exchanged phase. A similar behavior can be evidenced also in **1_lp** phase. Very likely this effect may be ascribed to the large hydration sphere that follows the Li insertion into the cavities. TG data confirm a higher water content of these phases with respect to the other ones (see the SI). Differently from Li- phases, the cell parameters of the Na- exchanged **1_np** phase are very similar to those of the **1_lp** phase suggesting that the insertion of Na^+ has the effect of opening the narrow pores of the phase **np**.

The differences among the phases can be seen, in a qualitative way, by looking at the separation of the first two reflections, namely the (110) and the (200), on their diffraction patterns (see Figure 9) which gives an idea of the variation of the channels size along the *a*- and *b*-axes when a cation is inserted.

Moreover, the insertion of metal ions into the cavities of **1** has also a remarkable influence on the global flexibility of the framework, acting as template.

As an example Figure 10 shows the TDXD patterns of H-phase **1_lp@H** (a) and the Li- phase **1_lp@Li** (b).

While for **1_lp@H** the framework undergoes several structural transformations due to water molecules loss (Figure 10a and c), for **1_lp@Li** the structural building remains stable up to about 120 °C when water is lost in a single step and the anhydrous phase is formed (Figure 10 b and d). Only a peak shifting around 80 °C due to the loss of a weakly bonded water molecule is observed. These observations are also confirmed by the TG curves in the SI. In addition, with respect to the H exchanged phases, the lp phases exchanged with metals do not show the phase transition toward a "np" phase after rehydration.

This is a further confirmation of the good ability of Li^+ and Na^+ to retain water into the cavities.

dx.doi.org/10.1021/ic3009656 | *Inorg. Chem.* 2012, 51, 6992−7000

Table 3. Refined Cell Parameters for 1_lp and 1_np Exchanged with 0.1 M Li, Na, and K Hydroxides[a]

	a/Å	b/Å	c/Å	β/°	V/Å^3
1_lp@Li	18.4582(9)	17.695(1)	8.0129(4)	93.29(0)°	2612.9(6)
1_lp@Na	18.923(1)	16.5046(7)	7.8437(3)	91.868(3)	2448.46(5)
1_lp@NH$_4$	18.5522(7)	17.049(1)	7.9491(4)	92.421(4)	2512.0(2)
1_lp@K	18.5656(6)	16.9054(8)	7.9218(4)	91.890(3)	2485.0(1)
1_np@Li	22.149(2)	15.067(1)	7.5684(7)	96.888(6)	2507.4(2)
1_np@Na	19.078(1)	16.4481(9)	7.8427(7)	92.090(6)	2458.88(2)
1_np@H	23.038(1)	13.1094(7)	7.6853(4)	98.349(3)	2296.5(1)

[a]Cell parameters of the H and NH$_4$ phases are also reported for comparison.

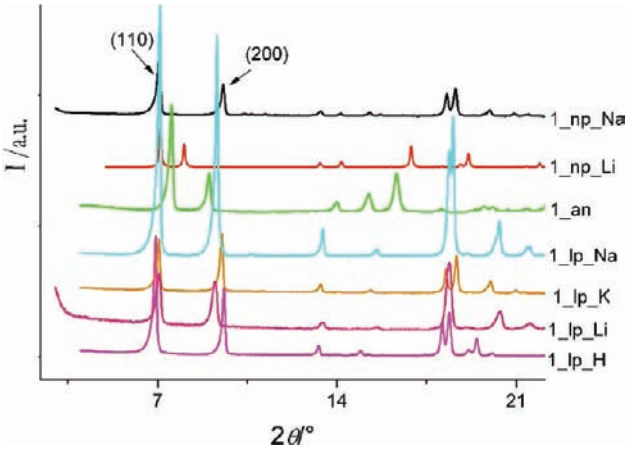

Figure 9. XRPD patterns of the exchanged phases of 1.

Lithium Insertion in Anhydrous Conditions. In order to avoid a solution mediated exchange mechanism that involves the large hydration sphere around Li^+ ions and that, very likely, limits the overall exchange capacity of the solid, Li ions have been also inserted into the cavites of **1_lp** by means of other two methods based on: (1) a high temperature solid state exchange with solid LiCl and (2) an exchange with LiBr dissolved in 3-hexanol.

For method 1, about 200 mg of preheated sample (140 °C for 12 h) has been ground in a crucible together with 100 mg (molar excess) of anhydrous LiCl powder. Then the solid mixture has been put in an oven and left standing for 3 days at 120 °C. Finally it has been washed twice in anhydrous ethanol in order to remove the unreacted Li chloride.

For method 2, about 200 mg of **1_lp@H** phase exchanged from water solution with Li^+ was heated at 130 °C for 12 h to completely dehydrate the sample. Then, it was contacted for 3 h with a saturated solution of LiBr in 3-hexanol, washed twice with THF in order to remove the adsorbed hexanol, and dried at air.

Procedure 1 was successful because ICP analysis indicates that about 2.7 mol of Li/mol of compound, corresponding to about 2.8 wt %, was taken by **1_lp** after this reaction whereas method 2 did not increase significantly the Li^+ uptake (Li/Zr molar ratio = 1.5, after the exchange). Despite the attempt to work in rigorous anhydrous conditions, TG curves (see Figure 3s) for the solid state exchanged phase indicate that, if left standing at air, a remarkable amount of water (about 20 and 25%, for methods 1 and 2, respectively) is retained inside the channels confirming the high hygroscopic behavior of the material containing Li.

Proton-Conduction Properties. The complex impedance ($Z^* = Z' + iZ''$) of **1_lp@H** pellet was measured as a function

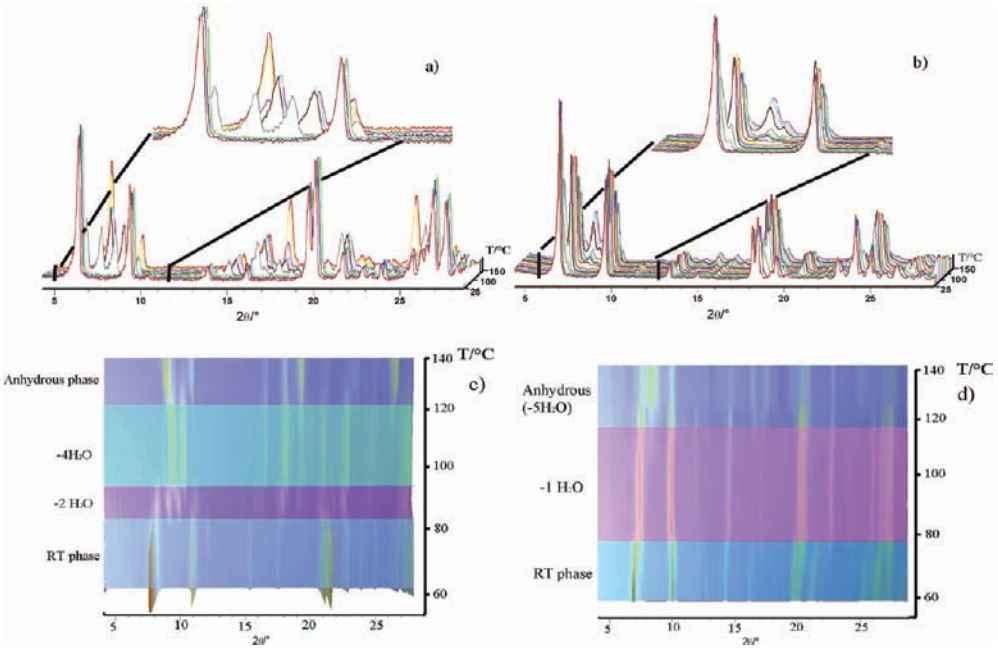

Figure 10. Comparison betweenTDXD plots of **1_lp@H** (a and c) and **1_lp@Li** (b and d) phases.

dx.doi.org/10.1021/ic3009656 | Inorg. Chem. 2012, 51, 6992−7000

of relative humidity (RH) at 70 °C (Figure 11). In the Nyquist plot representation (Z'' vs Z'), the frequency response of the

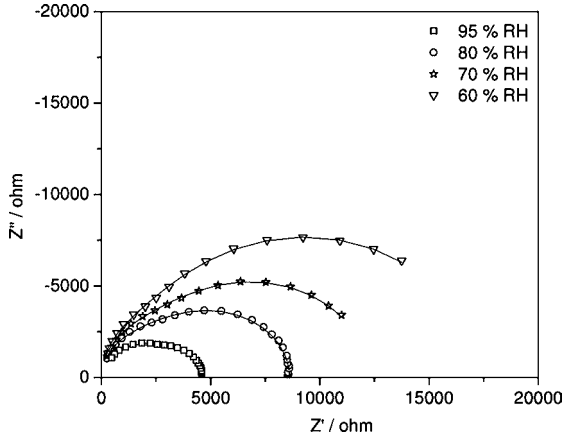

Figure 11. Nyquist plots for a polycrystalline sample of **1_lp@H** at 70 °C and at the indicate RH values. Solid lines are the fits of the impedance data to the equivalent circuit of Figure 12.

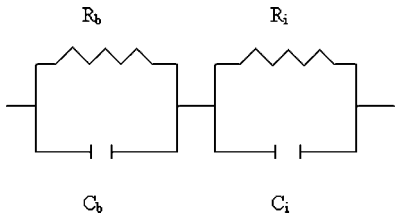

Figure 12. Equivalent circuit of a **1_lp@H** polycrystalline sample.

pellet consists in in two ill-separated semicircles (Figure 11). The response of the electrode–pellet interface does not appear in these plots since it lies outside the frequency range of the measurements. The overall resistance of the polycrystalline samples was obtained from arc extrapolation (R) to the Z' axis on the low frequency side (right side) of the Nyquist plot. The corresponding conductivity (σ) was calculated taking into account the thickness (d) and flat surface area (A) of the pellet: $\sigma = d/(RA)$.

The conductivity of the **1_lp@H** pellet changes from 1.3×10^{-5} to 4.9×10^{-5} S cm^{-1} when RH increases from 60% to 95%.

To get an insight into the physical origin of the conductivity, water uptake determinations were carried out at 70 °C in the RH range 60–95% according to ref 16. It was found that the material hydration (5.5 water molecules per unit formula) was independent of RH. Therefore the conductivity dependence on RH must arise from changes in the hydration of the particle surface and intergranular contacts.

The fact that the Nyquist plots consist of two ill-separated semicircles indicates that the frequency response of the pellet originates from two distinct transport processes. This is supported by the observation that the two semicircular portions of the Nyquist plots show different evolution with RH. Specifically, the low-frequency semicircle (on the right side of the Nyquist plot) grows more than the high-frequency semicircle (on the left side of the Nyquist plot) with decreasing RH at constant temperature.

Nyquist plots consisting in two ill-separated semicircles can be fitted to an equivalent circuit made of two resistance (R)/capacitance (C) parallel combinations connected in series and characterized by different time constants ($\tau = RC$).

For a polycrystalline system, the combination with the lower τ is usually associated with the bulk resistance (R_b) and the capacitance of the crystals, while the combination with the higher τ represents the resistance (R_i) and the capacitance of the interface between adjacent crystals. If this assignment is correct, then R_b should be independent of RH since the bulk hydration does not change with RH. The proposed equivalent circuit was able to simulate fairly accurately the frequency response of **1_lp@H** pellets as shown in Figure 11. Bulk (σ_b) and interfacial (σ_i) conductivities, calculated from R_b and R_i values, are plotted in Figure 13. In agreement with hydration data, σ_b is independent of RH within the error of the fit.

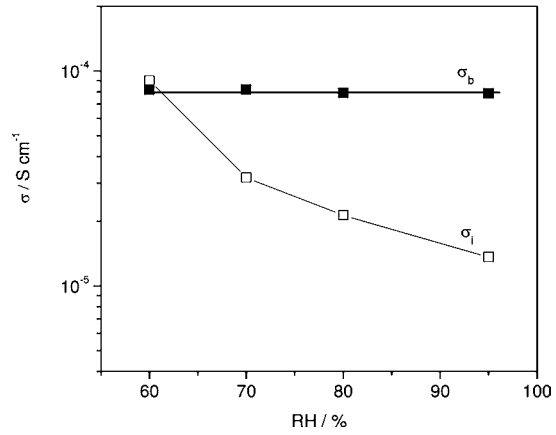

Figure 13. Bulk (σ_b) and interfacial (σ_i) conductivities, calculated from R_b and R_i values.

The complex impedance ($Z^* = Z' + iZ''$) of **1_lp@H** and **1_np@H** pellets was also measured as a function of the temperature at 95% RH. Nyquist plots of both materials are shown in Figures 14 and 15. The conductivity of the **1_lp@H** pellet changes from 2.6×10^{-5} to 5.4×10^{-5} S cm^{-1} when temperature increases from 30 to 80 °C (Figure 14). In the same range of temperature the conductivity of the **1_np@H** pellet increases from 1.5×10^{-6} to 6.6×10^{-6} S cm^{-1}. Since

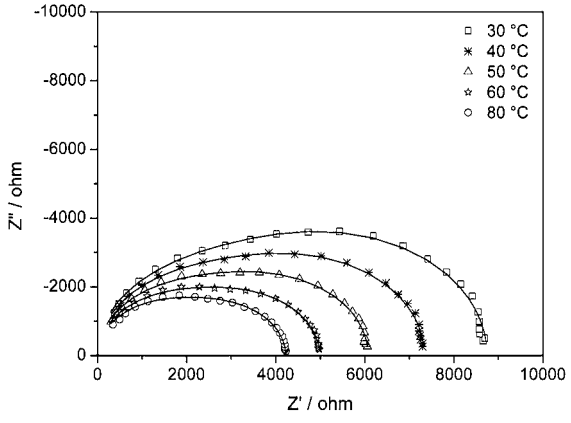

Figure 14. Nyquist plots for a polycrystalline sample of **1_lp@H** as a function of temperature at 95% RH. Solid lines are the fits of the impedance data to the equivalent circuit of Figure 12.

dx.doi.org/10.1021/ic3009656 | Inorg. Chem. 2012, 51, 6992–7000

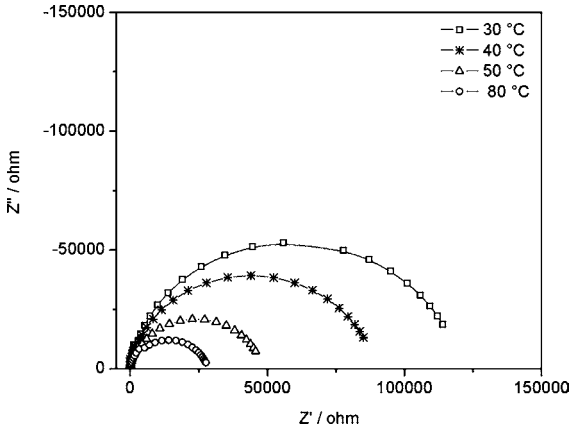

Figure 15. Nyquist plots for a polycrystalline sample of **1_np@H** as a function of temperature at 95% RH.

both materials have about the same surface area, it must be inferred that the higher conductivity of **1_lp@H**, arises from higher bulk conductivity.

Also in this case, the Nyquist plots of **1_np@H** consist of two ill-separated semicircles that can be fitted to the equivalent circuit of Figure 12.

Figure 16 shows the Arrhenius plot for bulk (σ_b) and interfacial (σ_i) conductivity calculated from R_b and R_i values, as well as for the overall pellet conductivity (σ).

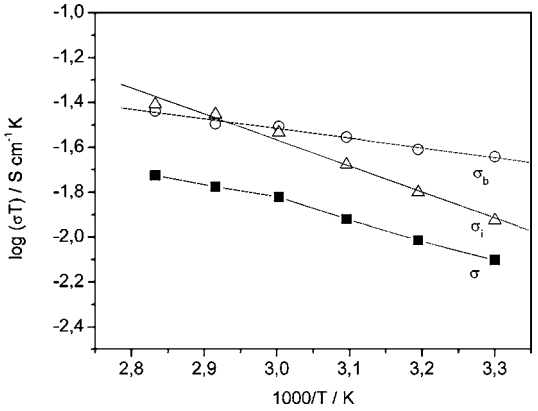

Figure 16. Arrhenius plot of bulk (σ_b), interfacial (σ_i), and overall (σ) conductivity for a polycrystalline sample of **1_lp@H**.

At the end of the experiments the pellets were checked by XRPD in order to test their stability and to exclude the occurrence of phase transitions. As result, the pellets were stable, no crystallinity loss occurred, and the phase **1_lp@H** did not convert into the **1_np@H** phases. The bulk conductivity (σ_b) ranges from 7.5×10^{-5} S cm^{-1} at 30 °C to 1.0×10^{-4} S cm^{-1} at 80 °C, being substantially comparable to the most part of other carboxylic MOF hydrated proton conductors recently reported.[7] The plots of $\log(\sigma_b T)$ and $\log(\sigma_i T)$ vs $1/T$ are linear and can be fitted to the equation $T\sigma = \sigma_0 \exp(-E_a/kT)$, where σ_0 is a pre-exponential factor and E_a, k, and T are, respectively, the apparent activation energy for conduction, Boltzmann's constant, and the absolute temperature. The activation energies for σ_b and σ_i are 0.09 and 0.23 eV, respectively, as determined from least-squares fits of the plots.

The Grotthuss and vehicle mechanisms have been proposed to interpret the proton conduction in solid compounds. The reported activation energies for the Grotthuss and vehicle mechanisms are in the ranges 0.1−0.4 and 0.5−0.9 eV, respectively.[17] Therefore, proton conduction in **1_lp@H** could be classified mainly as the Grotthuss mechanism. In addition, from structural analyses, the water molecules have been found to be trapped by strong hydrogen bonds in **1_lp@H** compound, so it seems difficult for the vehicle mechanism to occur in this system. Taking in account these conductivity values, the differences between **lp** and **np** phases could be due to a different disposition of the water molecules inside the channels. In fact, in both phases **1_lp** and **1_np**, a continuous path of H-bonded water molecule can be found by using the structural data. It should underlined that the water molecules have been found by using the difference Fourier calculations from powder data and therefore the uncertainty on their position is higher than structure determination from single crystal diffraction data. However, the observed bond lengths can give useful hints for a better understanding of the conductivity data. For phase **1_lp**, the H-bonds are stronger, being comprised in the range 2.4−2.5 Å, and with two possible paths at least, whereas for phase **1_np** the observed H-bonds are weaker, monodirectional, and the with a partial occupancy of the water molecules.

These observations are depicted in Figure 17.

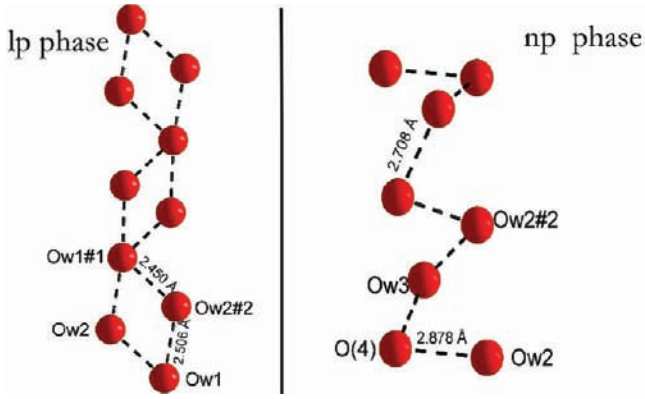

Figure 17. H-bond paths for **1_lp** and **1_np** phases. Symmetry codes: no. 2 = $-x$, $+y$, $-z + {}^1/_2$.

CONCLUSION

The zirconium tetraphosphonate **1** has been studied for its structural, ion- exchange, and conduction properties. The structural flexibility, induced by thermal treatment and successive rehydration, has important consequences on its properties owing to the formation of new H-bonds and to a different disposition of water clusters into the channels. The latter has been deeply studied by using TDXD coupled with Rietveld refinements, giving a full explanation of the transformation mechanisms. The ion exchange behavior is strongly influenced by the opening of the pores and by the hydration sphere of the exchanged ions. As a matter of fact, Li^+ exchanged phases have the higher water content respect to the H^+, Na^+, and K^+ phases. To increase the uptake of Li^+ ion a different methods of exchange in anhydrous conditions has been used. This method was successful because up to nearly 3 mol of Li^+ /mol of compounds can be exchanged in this way. Finally, an accurate study on the proton conductivity of **1** at different temperatures and humidity has been done and the different

dx.doi.org/10.1021/ic3009656 | Inorg. Chem. 2012, 51, 6992−7000

contributions of the interfacial and bulk conductivity have been calculated by fitting the impedance data to a suitable equivalent circuit. Actually, similar Zr coordination polymers containing other organic spacer are under preparation. Owing to their very high chemical stability, these compounds could be subjected to several post synthetic treatments in protic solvents with high acidity and basicity, thus affording new unexpected features and applications in the material sciences.

■ ASSOCIATED CONTENT

Supporting Information

Crystallographic information file in cif format for the **1_np@H** phase. Structural parameters and tables for the phase **1_np@H**, thermogravimetric data, detailed Rietveld plots, and procedures for the fitting of the impedance plots. This material is available free of charge via the Internet at http://pubs.acs.org or from the Authors.

■ AUTHOR INFORMATION

Corresponding Author

*E-mail: fcost@unipg.it. Fax: +390755855566.

Present Address

[§]Institute for Membrane Technology (ITM-CNR), Via Pietro BUCCI, Cubo 17c, 87030 Rende, Cs, Italy.

Notes

The authors declare no competing financial interest.

■ REFERENCES

(1) (a) Kitagawa, S.; Matsuda, R. *Coord. Chem. Rev.* **2007**, *251*, 2490. (b) Llewellyn, P. L.; Bourrelly, S.; Serre, C.; Filinchuk, Y.; Férey, G. *Angew. Chem., Int. Ed.* **2006**, *45*, 7751. (c) Kubota, Y.; Takata, M.; Matsuda, R.; Kitaura, R.; Kitagawa, S.; Kobayashi, T. C. *Angew. Chem., Int. Ed.* **2006**, *45*, 4932. (d) Kondo, A.; Noguchi, H.; Carlucci, L.; Proserpio, D. M.; Ciani, G.; Kajiro, H.; Ohba, T.; Kanoh, H.; Kaneko, K. *J. Am. Chem. Soc.* **2007**, *129*, 12362.

(2) (a) Tanaka, D.; Nakagawa, K.; Higuchi, M.; Horike, S.; Kubota, Y.; Kobayashi, T. C.; Takata, M.; Kitagawa, S. *Angew. Chem., Int. Ed.* **2008**, *120*, 3978. (b) Tanaka, D.; Henke, A.; Albrecht, A.; Moeller, M.; Nakagawa, K.; Kitagawa, S.; Groll, S. *Nature Chem.* **2010**, *2*, 410. (c) Millange, F.; Serre, C.; Guillou, N.; Ferey, G.; Walton, R. I. *Angew. Chem., Int. Ed.* **2008**, *47*, 4100. (d) Serre, C.; Mellot-Draznieks, C.; Surblé, S.; Audebrand, N.; Filinchuk, Y.; Férey, G. *Science* **2005**, *315*, 1828.

(3) (a) Deng, H.; Doonan, C. J.; Furukawa, H.; Ferreira, R. B.; Towne, J.; Knobler, C. B.; Wang, B.; Yaghi, O. M. *Science* **2010**, *327* (5967), 846. (b) Henke, S.; Fischer, R. A. *J. Am. Chem. Soc.* **2011**, *133* (7), 2064. (c) Custelcean, R.; Gorbunova, M. G. *J. Am. Chem. Soc.* **2005**, *127* (47), 16362. (d) Horcajada, P.; Salles, F.; Wuttke, S.; Devic, T.; Heurtaux, D.; Maurin, G.; Vimont, A.; Daturi, M.; David, O.; Magnier, E.; Stock, N.; Filinchuk, Y.; Popov, D.; Riekel, C; Férey, G.; Serre, C. *J. Am. Chem. Soc.* **2011**, *133* (44), 17839.

(4) (a) Maji1, T. K.; Matsuda, R.; Kitagawa, S. *Nat. Mater.* **2007**, *6*, 142. (b) Tanabe, K. K.; Cohen, S. M. *Chem. Soc. Rev.* **2011**, *40*, 498 and references therein. (c) Song, Y.; Cronin, L. *Angew. Chem., Int. Ed.* **2008**, *47*, 4635. (d) Wang, Z.; Cohen, S. M. *J. Am. Chem. Soc.* **2007**, *129* (41), 12368.

(5) (a) Meek, S. T.; Greathouse, J. A.; Allendorf, M. D. *Adv. Mater.* **2011**, *23*, 249. (b) Lee, J.; Farha, O- K.; Roberts, J.; Scheidt, K. A.; Nguyen, S. T.; Hupp, J. T. *Chem. Soc. Rev.* **2009**, *38*, 1450. (c) Kupplera, R. J.; Timmonsb, D. J.; Fanga, Q.; Lia, J.; Makala, T. A.; Younga, M. D.; Yuana, D.; Zhaoa, D.; Zhuanga, W.; Zhou, H. *Coord. Chem. Rev.* **2009**, *253*, 3042 and references therein. (d) Chen, B.; Xiang, S.; Qian, G. *Acc. Chem. Res.* **2010**, *43* (8), 1115. (e) An, J.; Rosi, N. L. *J. Am. Chem. Soc.* **2010**, *132* (16), 5578.

(6) (a) Shigematsu, A.; Yamada, T.; Kitagawa, H. *J. Am. Chem. Soc.* **2011**, *133* (7), 2034. (b) Volkringer, C.; Loiseau, V.; Guillou, V; Férey, G.; Haouas, M.; Taulelle, F.; Elkaim, V.; Stock, N. *Inorg. Chem.* **2010**, *49* (21), 9852.

(7) (a) Sahoo, S. C.; Kundu, T.; Banerjee, R. *J. Am. Chem. Soc.* **2011**, *133*, 17950. (b) Shigematsu, A.; Yamada, T.; Kitagawa, H. *J. Am. Chem. Soc.* **2011**, *133*, 2034. (c) Jeong, N. C.; Samanta, B.; Lee, C. Y.; Farha, O. K.; Hupp, J. T. *J. Am. Chem. Soc.* **2012**, *134* (1), 51. (d) Umeyama, D.; Horike, S.; Inukai, M.; Hijikata, Y; Kitagawa, S. *Angew. Chem., Int. Ed.* **2011**, *50*, 1. (e) Taylor, J. M.; Mah, R. K.; Moudrakovski, I. L.; Ratcliffe, C. I.; Vaidhyanathan, R.; Shimizu, G. K. H. *J. Am. Chem. Soc.* **2010**, *132*, 14055.

(8) (a) Groves, J. A.; Miller, S. R.; Warrender, S. J.; Mellot-Draznieks, C.; Lightfoot, P.; Wright, P. A. *Chem. Commun.* **2006**, *31*, 3305. (b) Wharmby, M. T.; Mowat, J. P. S.; Thompson, S. P.; Wright, P. A. *J. Am. Chem. Soc.* **2011**, *133* (5), 1266. (c) Serre, C.; Groves, J. A.; Lightfoot, P.; Slawin, A. M. Z.; Wright, P. A.; Stock, N.; Bein, T.; Haouas, M.; Taulelle, F.; Ferey, G. *Chem. Mater.* **2006**, *18* (6), 1451. (d) Miller, S. R.; Pearce, G. M.; Wright, P. A.; Bonino, F.; Chavan, S.; Bordiga, S.; Margiolaki, I.; Guillou, N.; Ferey, G.; Bourrelly, S.; Llewellyn, P. L. *J. Am. Chem. Soc.* **2008**, *130* (47), 15967.

(9) (a) Vivani, R.; Alberti, G.; Costantino, F.; Nocchetti, M. *Microporous Mesoporous Mater.* **2008**, *107*, 58. (b) Costantino, U.; Nocchetti, M.; Vivani, R. *J. Am. Chem. Soc.* **2002**, *124*, 8428. (c) Vivani, R.; Costantino, U.; Nocchetti, M. *J. Mater. Chem.* **2002**, *12*, 3254. (d) Casciola, M.; Capitani, D.; Donnadio, A.; Diosono, V.; Piaggio, P.; Pica, M. *J. Mater. Chem.* **2008**, *18*, 4291. (e) Casciola, M.; Capitani, D.; Donnadio, A.; Frittella, V.; Pica, M.; Sganappa, M. *Fuel Cells* **2009**, *9*, 381.

(10) Cagnon, K. J.; Perry, H. P.; Clearfield, A. *Chem. Rev.* **2012**, *112* (2), 1034 and ref. therein..

(11) Vivani, R.; Costantino, U.; Nocchetti, M.; Costantino, F. *Inorg. Chem.* **2006**, *45*, 2388.

(12) Moedritzer, K.; Irani, R. R. *J. Org. Chem.* **1966**, *31*, 1603.

(13) Alberti, G.; Casciola, M.; Massinelli, L.; Bauer, B. *J. Membr. Sci.* **2001**, *185*, 73−81.

(14) Werner, P. E.; Eriksson, L.; Westdhal, M. *J. Appl. Crystallogr.* **1985**, *18*, 367.

(15) Larson, C.; von Dreele, R. B. *Generalized Crystal Structure Analysis System*; Los Alamos National Laboratory: Los Alamos, NM, 2001.

(16) Donnadio, A.; Casciola, M.; Di Vona, M. L.; Tamilvanan, M. *J. Power Sources* **2012**, *205*, 145.

(17) Colomban, P. Proton Conductors: Solids, Membranes and Gels - Materials and *Devices. Chemistry of Solid State Materials*; Cambridge University Press: Cambridge, U.K., 1992; Vol. *2*.